Available online at www.sciencedirect.com
ScienceDirect
Composites Science and Technology 68 (2008) 1688–1696
COMPOSITES SCIENCE AND TECHNOLOGY
www.elsevier.com/locate/compscitech

Anisotropic creep modeling of coated textile membrane using finite element analysis

Kyoung Ju Kim [a], Woong-Ryeol Yu [a,*], Min Sun Kim [b]

[a] Department of Materials Science and Engineering, Seoul National University, Shillim-dong, Kwanak-gu, Seoul 151-744, South Korea
[b] Textile Research Team, Korea Institute of Industrial Technology, Cheonan, South Korea

Received 3 August 2007; received in revised form 17 December 2007; accepted 6 February 2008
Available online 15 February 2008

Abstract

Coated textile membranes (CTMs) form a class of flexible textile composites undergoing viscoelastic deformation because they consist of a polymeric reinforcement and matrix and are tensioned in service. In most CTMs, woven fabrics are frequently used as a reinforcement structure, causing anisotropic mechanical behavior including time dependent viscoelastic deformation. To describe such anisotropic and nonlinear time dependent deformation, the creep potential with three orthotropic parameters was introduced and incorporated into finite element software through a user material subroutine. The three parameters included in the creep potential were determined by carrying out off-axis coupon creep tests and using various mathematical formulae for the effective creep compliance. To validate the current creep modeling and its implementation in finite element software, off-axis coupon creep tests were re-simulated and compared with the experiments, showing that the present modeling can describe the anisotropic and nonlinear creep deformation of CTM with acceptable accuracy.

Keywords: A. Flexible composites; B. Creep; B. Non-linear behavior; C. Anisotropy; C. Finite element analysis (FEA)

1. Introduction

Coated textile membranes (CTMs) form a class of flexible textile composites that are used for moderate span enclosures (roofs and air-halls), where their properties of lightness, high tensile strength, durability and fire resistance may be exploited [1]. CTMs are tensioned in multi-axial directions to form complex shapes in which they are maintained for a considerable period of time (see Fig. 1). Due to the polymeric nature of the coating materials and fabric reinforcements used in them, CTMs deform in a time dependent manner when they are subjected to a constant stress. Such a viscoelastic deformation becomes more pronounced when the CTM is more highly stressed or exposed to elevated temperatures. Since the CTM is tensioned in multi-axial directions, it is expected to undergo creep deformation, which may cause unfavorable dimensional changes, deteriorated structural performance and, in the worst case, material failure. Thus, viscoelastic deformation, especially creep deformation, should be analyzed to prevent such defects from arising in CTMs.

Over the course of the past several decades, many studies have been conducted to formulate the time dependent viscoelastic deformation. If considered in terms of the methodology employed, these studies can be classified into the two main approaches. The first approach is called 'an equation of state' formulation [2]. It relies on the assumption that the response of the material explicitly depends on its present state or the material remembers its past explicitly and responds to the present in a manner that reflects its past history. Sun et al. [3–5] studied the creep behavior of uniaxial fiber reinforced plastic (FRP) composites, in which continuous fibers were reinforced in one direction in the laminae. They adopted a quadratic plastic potential to model the anisotropic creep behavior, defining the effective stress and creep strain rate which are adequate for analyzing the creep behavior of composites in the multi-axial

* Corresponding author. Tel.: +82 2 880 9096; fax: +82 2 883 8197.
E-mail address: woongryu@snu.ac.kr (W.-R. Yu).

0266-3538/$ - see front matter © 2008 Elsevier Ltd. All rights reserved.
doi:10.1016/j.compscitech.2008.02.011

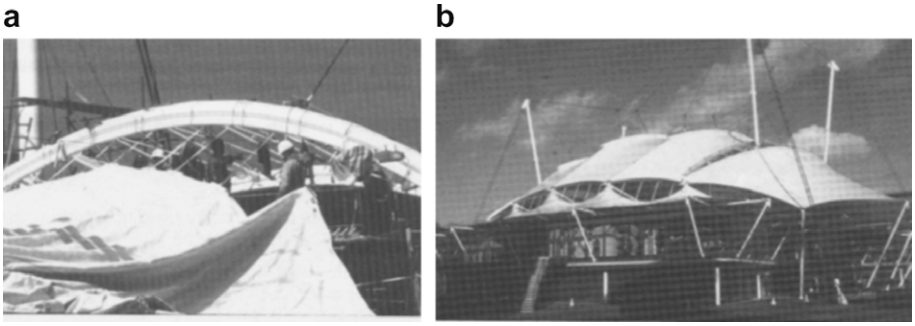

Fig. 1. Application of a CTM for a roof structure [1]. (a) Before stressing; (b) after stressing.

stress state. The second approach is the so-called 'memory' approach using the hereditary integral. This approach claims that materials remember their past explicitly and respond to the present reflecting their past history. There are many literatures which discuss this memory approach, e.g., [6–8]. For nonlinear viscoelastic deformation analysis, Schapery [9] derived a single integral type of constitutive equation from thermodynamic principles several decades ago. Recently, the Schapery equation has been utilized to analyze the nonlinear viscoelastic behavior of composites, e.g., [10] for carbon/epoxy composites, [11] for thermoplastic/agro-fiber composites, and [12] for the viscoelastic analysis of pultruded composite materials, etc [13,14].

In this work, the first approach, i.e., 'an equation of state' formulation approach was used to describe the creep behavior of CTMs. The creep potential and its numerical formulation were implemented in finite element software (here ABAQUS) through a user material subroutine. A brief explanation of the background theory of creep deformation will be given in the following section and the characterization method and validation example will be discussed.

2. Theoretical background

This study adopts so-called 'equation of state' approach, which relies on the assumption that the response of the material depends on its present state explicitly and thus the creep strain can be calculated through the creep potential with the current stress. The orthotropic creep potential was used because polymeric woven reinforcements in CTMs tend to show the orthotropic mechanical behavior. The main source of the orthotropic anisotropy in woven fabrics can be found in the weaving process, in which the warp yarns are tensioned, thus causing them to experience friction with the weft yarns. This tension and resulting friction result in anisotropy, i.e., the mechanical stiffness of the woven fabric in the warp direction is generally stronger than that in the weft direction.

2.1. Creep potential

The creep potential can be defined as the potential that can predict the creep strain rate based on the current stress state. To determine the creep potential for CTMs, we first need to consider the components of the CTM and their mechanical behavior. The polymeric fibers used in CTMs are not as rigid as carbon or graphite fibers and, therefore, they are likely to deform in a time dependent manner when a constant load is applied, while carbon or glass fibers in advanced composites can be assumed to undergo no deformation under a constant load. Therefore, for a CTM with polymeric fibers, the following potential is introduced that can describe the creep deformation in the fiber directions.

$$f = \sqrt{\frac{1}{2}(a_{11}\sigma_{11}^2 + \sigma_{22}^2 + 2a_{66}\sigma_{12}^2 + 2a_{12}\sigma_{11}\sigma_{22})} = \bar{\sigma} \tag{1}$$

where a_{11}, a_{66} and a_{12} are unknown material parameters, while σ_{ij} represents the current stresses. Note that the effective stress ($\bar{\sigma}$) is defined to be the same as the creep potential itself. This potential was used to model the orthotropic elastic–plastic deformation of boron/aluminum composite [15], based on the theory of plasticity for sheet metals [16]. In the present study, the same potential is used to model the anisotropic creep behavior of a CTM in the multi-axial stress state. The creep strain rates ($\dot{\boldsymbol{\varepsilon}}^{c}$ or $\dot{\varepsilon}_{ij}^{c}$) can be calculated using the flow rule, as in the case of the plasticity

$$\dot{\boldsymbol{\varepsilon}}^{c} = \dot{\lambda}\frac{\partial f}{\partial \boldsymbol{\sigma}} \quad \text{or} \quad \begin{pmatrix} \dot{\varepsilon}_{11}^{c} \\ \dot{\varepsilon}_{22}^{c} \\ 2\dot{\varepsilon}_{12}^{c} \end{pmatrix} = \frac{\dot{\lambda}}{2f}\begin{bmatrix} a_{11}\sigma_{11} + a_{12}\sigma_{22} \\ \sigma_{22} + a_{12}\sigma_{11} \\ 2a_{66}\sigma_{12} \end{bmatrix} \tag{2}$$

where $\dot{\lambda}$ is a scale factor. The total strain rate now becomes,

$$\dot{\varepsilon}_{ij} = \dot{\varepsilon}_{ij}^{e} + \dot{\varepsilon}_{ij}^{c} \tag{3}$$

where the elastic strains ε_{ij}^{e} are assumed to occur instantaneously as the load is applied. To determine the unknown parameters in Eq. (1), it is essential to employ the concept of the effective stress and effective strain rate in a similar way to that employed in [3,15]. The effective strain rate conjugate to the effective stress can be defined by introducing the rate of work done, i.e.,

$$\dot{W}^{c} = \sigma_{ij}\dot{\varepsilon}_{ij}^{c} = \bar{\sigma}\bar{\dot{\varepsilon}}^{c}, \tag{4}$$

resulting in the effective creep strain rate as follows:

$$\bar{\dot{\varepsilon}}^{c} = \dot{\lambda} = \sqrt{\frac{2}{(a_{11}-a_{12}^2)}}\sqrt{(\dot{\varepsilon}_{11}^{c})^2 + a_{11}(\dot{\varepsilon}_{22}^{c})^2 + \frac{2(a_{11}-a_{12}^2)}{a_{66}}(\dot{\varepsilon}_{12}^{c})^2 - 2a_{12}(\dot{\varepsilon}_{11}^{c})(\dot{\varepsilon}_{22}^{c})} \tag{5}$$

The unknown parameters (a_{11}, a_{66}, a_{12}) in the potential can be determined using the uniaxial off-axis coupon test results. Note that the warp direction in the CTM is the '1' direction, and the weft direction is the '2' direction. The stress (σ_θ) at an off-axis direction can be measured using the off-axis coupon test. This off-axis stress can be transformed to the 1–2 coordinate system and, using Eq. (1), the effective stress can be expressed by

$$\bar{\sigma} = H(\theta)\sigma_\theta \tag{6}$$

where
$H(\theta) = \sqrt{\frac{1}{2}(a_{11}\cos^4\theta + \sin^4\theta + 2(a_{66}+a_{12})\cos^2\theta\sin^2\theta)}$.

The effective creep strain rate can be calculated from the off-axis strain rate as follows:

$$\bar{\dot{\varepsilon}}^{c} = \frac{\dot{\varepsilon}_\theta^{c}}{H(\theta)}, \quad \bar{\varepsilon}^{c} = \frac{\varepsilon_\theta^{c}}{H(\theta)} \tag{7}$$

Note that Eq. $(7)_2$ is obtained by integrating $(7)_1$ with the proportional loading assumption. Then, the effective creep compliance may be defined as in [4]

$$\overline{J} = \frac{\bar{\varepsilon}^{c}}{\bar{\sigma}} = \frac{\varepsilon_\theta^{c}/H(\theta)}{H(\theta)\sigma_\theta} = \frac{\varepsilon_\theta^{c}}{\sigma_\theta}\frac{1}{H^2(\theta)} = \frac{J_\theta}{H^2(\theta)} \tag{8}$$

where J_θ is the creep compliance in the θ direction. Note that the effective creep compliance can be represented by the axial creep compliance (J_θ) and $H(\theta)$ and, furthermore, the effective creep compliance in the different off-axis directions can be collapsed into a single master curve if the unknown parameters (a_{11}, a_{66}, a_{12}) are properly determined. Therefore, it can be concluded that the procedure used for determining the unknown parameters is equivalent to finding the values of a_{11}, a_{66} and a_{12} that allow all of the effective creep compliances obtained from each off-axis test to be collapsed onto the same curve. In previous papers [3–5,17,18], a trial-and-error method was used to accomplish this, however, in the current study, a systematic method is developed by defining an objective function as follows:

$$\Phi(a_{11},\tilde{a}_{22}) = \sum_{t=1}^{n}\left\{\left(\frac{2J_0^t}{3a_{11}} - \frac{2J_{90}^t}{3}\right)^2 + \left(\frac{2J_{90}^t}{3} - \frac{J_{45}^t}{H^2(45^\circ)}\right)^2 + \left(\frac{J_{45}^t}{H^2(45^\circ)} - \frac{2J_0^t}{3a_{11}}\right)^2\right\} \tag{9}$$

where the superscript (t) associated with the off-axis creep compliance (J_θ) denotes the time step, and $\tilde{a}_{22} = a_{66} + a_{12}$. Since the objective function represents the differences between the effective creep compliance measured from each off-axis coupon test, the parameter set that minimizes the function may ensure that all of the effective creep compliances collapse on a single curve [19]. A simplex minimization algorithm in MATLAB was used in this study.

2.2. Numerical integration algorithm

A stress integration (or update) algorithm is necessary for implementing the creep constitutive equation in finite element software. For this purpose, the creep constitutive equation is firstly summarized

$$\dot{\boldsymbol{\varepsilon}}^{c} = \bar{\dot{\varepsilon}}^{c}\frac{\partial\bar{\sigma}}{\partial\boldsymbol{\sigma}}, \quad \bar{\dot{\varepsilon}}^{c} = \varphi(\bar{\sigma},\bar{\varepsilon}^{c}), \quad \dot{\boldsymbol{\sigma}} = \mathbf{C}\cdot\dot{\boldsymbol{\varepsilon}}^{e} = \mathbf{C}\cdot(\dot{\boldsymbol{\varepsilon}} - \dot{\boldsymbol{\varepsilon}}^{c}) \tag{10}$$

where $\dot{\boldsymbol{\varepsilon}}^{c}$, $\bar{\dot{\varepsilon}}^{c}$ and $\dot{\boldsymbol{\varepsilon}}^{e}$ are the creep strain rate, the effective creep strain rate, and the elastic strain rate, respectively. Note that $\mathbf{C}$ is the orthotropic elastic stiffness matrix. Eq. $(10)_2$ is a creep equation determined experimentally, relating the effective creep strain and stress to the effective creep strain rate. For the time stepping, $\boldsymbol{\sigma}_n, \boldsymbol{\varepsilon}_n, \boldsymbol{\varepsilon}_n^{c}$ and $\bar{\varepsilon}_n^{c}$ at time step t_n are assumed to be given with a strain increment ($\Delta\boldsymbol{\varepsilon}$) for the next time step ($t_{n+1} = t_n + \Delta t$). A stress integration method [20,21] is used to evaluate the stress at the next time step, satisfying the assumption that the creep deformation occurs in the normal direction to the creep potential. The Euler backward scheme [20] was utilized in the current work, resulting in the equation:

$$\begin{aligned}&\boldsymbol{\varepsilon}_{n+1}^{c} = \boldsymbol{\varepsilon}_n^{c} + \Delta\bar{\varepsilon}_{n+1}\frac{\partial\bar{\sigma}}{\partial\boldsymbol{\sigma}_{n+1}},\\ &\Delta\bar{\varepsilon}_{n+1} = \Delta t\dot{\bar{\varepsilon}} = \Delta t\varphi(\boldsymbol{\sigma}_{n+1},\bar{\varepsilon}_{n+1}), \quad \boldsymbol{\sigma}_{n+1} = \mathbf{C}\cdot(\boldsymbol{\varepsilon}_{n+1} - \boldsymbol{\varepsilon}_{n+1}^{c})\end{aligned} \tag{11}$$

Note that the subscript represents the time step. Since the flow rule for creep strain dictates that the creep strain increment or strain rate is normal to the effective stress surface (or creep potential), an iteration scheme needs to be developed, for which an objective function is introduced as follows:

$$\mathbf{R} = -\boldsymbol{\varepsilon}^{c} + \boldsymbol{\varepsilon}_n^{c} + \Delta\bar{\varepsilon}_{n+1}\frac{\partial\bar{\sigma}}{\partial\boldsymbol{\sigma}_{n+1}} \tag{12}$$

Then, the linearization of the above equation results in,

$$\mathbf{R}^{(k)} - \Delta\boldsymbol{\varepsilon}_{n+1}^{c(k)} + \delta(\Delta\bar{\varepsilon}_{n+1}^{(k)})\frac{\partial\bar{\sigma}}{\partial\boldsymbol{\sigma}_{n+1}^{(k)}} + \Delta\bar{\varepsilon}_{n+1}^{(k)}\frac{\partial^2\bar{\sigma}}{\partial\boldsymbol{\sigma}_{n+1}^{(k)}\partial\boldsymbol{\sigma}_{n+1}^{(k)}}\cdot\Delta\boldsymbol{\sigma}^{(k)} = 0 \tag{13}$$

Note that the superscript k indicates the iteration step. Finally, the increment of the effective creep strain is obtained by,

$$\delta(\Delta\bar{\varepsilon}_{n+1}^{(k)}) = \frac{-\Delta t\varphi_{\boldsymbol{\sigma}_{n+1}^{(k)}}\cdot\widetilde{\mathbf{C}}\cdot\mathbf{R}^{(k)}}{1 + \Delta t\varphi_{\boldsymbol{\sigma}_{n+1}^{(k)}}\cdot\widetilde{\mathbf{C}}\cdot\mathbf{m}_{n+1}^{(k)} - \Delta t\varphi_{\bar{\varepsilon}_{n+1}^{(k)}}} \tag{14}$$

where

$$\mathbf{m}_{n+1}^{(k)} = \frac{\partial \bar{\sigma}}{\partial \boldsymbol{\sigma}_{n+1}^{(k)}}, \quad \mathbf{M}_{n+1}^{(k)} = \frac{\partial^2 \bar{\sigma}}{\partial \boldsymbol{\sigma}_{n+1}^{(k)} \partial \boldsymbol{\sigma}_{n+1}^{(k)}},$$
$$\widetilde{\mathbf{C}}^{-1} = (\mathbf{C}^{-1} + \Delta\bar{\varepsilon}_{n+1}^{(k)} \mathbf{M}_{n+1}^{(k)}) \tag{15}$$

Then, the stress increment and creep strain increment are obtained as follows

$$\Delta\boldsymbol{\sigma}_{n+1}^{(k)} = -\widetilde{\mathbf{C}} \cdot \mathbf{R}^{(k)} - \delta\left(\Delta\bar{\varepsilon}_{n+1}^{(k)}\right) \widetilde{\mathbf{C}} \cdot \mathbf{m}_{n+1}^{(k)},$$
$$\Delta\boldsymbol{\varepsilon}_{n+1}^{c(k)} = -\mathbf{C}^{-1} \cdot \Delta\boldsymbol{\sigma}_{n+1}^{(k)} \tag{16}$$

Finally, the stress and strain quantities at the next time step, $t_{n+1} = t_n + \Delta t$, are updated as follows:

$$\boldsymbol{\sigma}_{n+1}^{(k+1)} = \boldsymbol{\sigma}_{n+1}^{(k)} + \Delta\boldsymbol{\sigma}_{n+1}^{(k)},$$
$$\boldsymbol{\varepsilon}_{n+1}^{c(k+1)} = \boldsymbol{\varepsilon}_{n+1}^{c(k)} + \Delta\boldsymbol{\varepsilon}_{n+1}^{c(k)}, \quad \Delta\bar{\varepsilon}_{n+1}^{(k+1)} = \Delta\bar{\varepsilon}_{n+1}^{(k)} + \delta(\Delta\bar{\varepsilon}_{n+1}^{(k)}) \tag{17}$$

Eqs. (14)–(17) are repeated until the creep strain increment is found to be normal to the creep potential. The tangent stiffness can be also derived through the linearization of the constitutive equation in Eq. (11) as follows:

$$\frac{\partial\boldsymbol{\sigma}_{n+1}}{\partial\boldsymbol{\varepsilon}_{n+1}} = \left(\widetilde{\mathbf{C}} - \frac{(\Delta t)\widetilde{\mathbf{C}} \cdot \mathbf{m}_{n+1} \otimes \varphi_{\boldsymbol{\sigma}_{n+1}} \cdot \widetilde{\mathbf{C}}}{1 + (\Delta t)\varphi_{\boldsymbol{\sigma}_{n+1}} \cdot \widetilde{\mathbf{C}} \cdot \mathbf{m}_{n+1} - (\Delta t)^2 \varphi_{\bar{\varepsilon}_{n+1}}} \right). \tag{18}$$

3. Results and discussion

3.1. Material characterization

A textile membrane reinforced with poly (ethylene terephthalate) fabric reinforcement was used in this study. The fabric structure of the reinforcement was plain weave (28 wpi × 26 ppi), in which the yarns finenesses were 1500 and 1000 denier for the warp and weft yarns, respectively. The coating matrix was poly (vinyl chloride) with poly (vinylidene fluoride) as a topping material for ultraviolet protection. The coated textile membrane was 1.15 mm thick.

Both uniaxial tension and creep tests were conducted using a Dynamic Mechanical Analysis (DMA) tester (TA Q800). The temperature was fixed at 30 °C for all of the tests. To take into account the anisotropic material properties, off-axis coupon specimens were prepared with sizes of 8 mm in width by 12 mm in length by cutting the CTM at angles of 0°, 45°, and 90° from the warp direction. As shown in Fig. 2, orthotropic anisotropy was exhibited due to the woven reinforcement, i.e., the warp direction is most resistant to deformation, followed by the weft and bias directions in that order. The time-independent elastic moduli in each direction were determined from the initial slope of the stress and strain curves (see Table 1). In this study Poisson's ratio was assumed while the shear modulus was calculated using the measured modulus in the 45° direction and the following equation

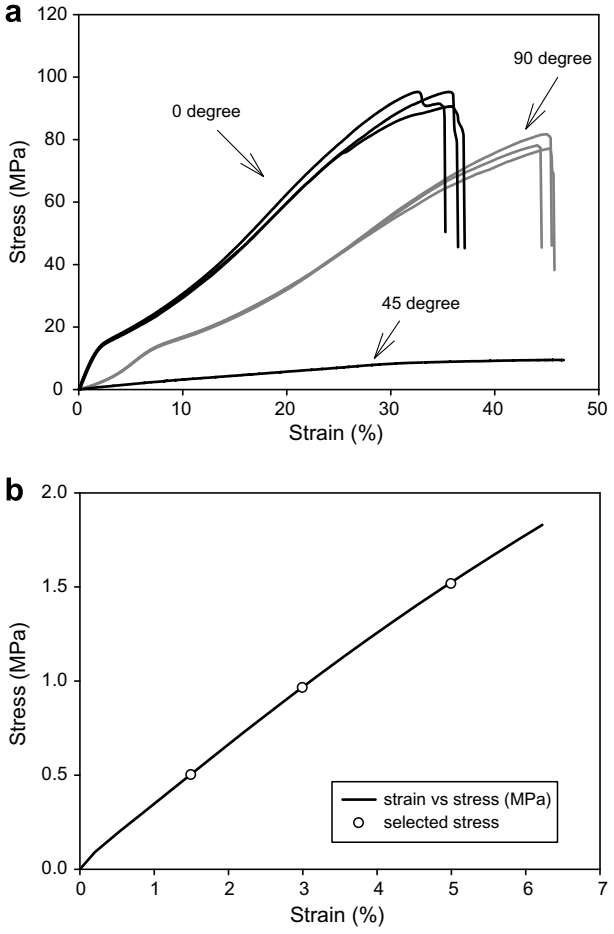

Fig. 2. Stress and strain curves of CTM from uniaxial tension test; (a) 0°, 45° and 90° off-axis; (b) magnified plot of 45° off-axis test.

Table 1
Time-independent elastic moduli of a CTM

E_{11} (MPa) (warp)	E_{22} (MPa) (weft)	G (MPa) (shear)	v	E_{45} (MPa) (bias)
223	58	7.3	0.3	26

$$\frac{1}{E_\theta} = \frac{\cos^4\theta}{E_1} + \left(\frac{1}{G} - \frac{2v}{E_1}\right)\cos^2\theta\sin^2\theta + \frac{\sin^4\theta}{E_2} \tag{19}$$

where E_θ, G, and v are the tensile modulus in the θ direction, the shear modulus, and Poisson's ratio, respectively, while E_1 and E_2 are the tensile modulus in the material direction of the orthotropic material, respectively. Since the bias direction is more compliant than the other two directions, the load level for the creep tests was determined based on the 45° direction test. Three different load levels (0.5, 0.9630 and 1.5150 MPa) corresponding to 1.5%, 3.0% and 5.0% strains, respectively, were chosen, as shown in Fig. 2b. Then, the creep strains were measured for 300 min under these three load levels (see Fig. 3). As expected, the creep strain increased as the load level increased. The creep resistance in the bias direction is less

than that in the other directions, which is consistent with the results of the tensile test. Note that the woven structure has two preferred fiber directions (the warp (0°) and weft (90°) directions), implying that the amount of aligned fibers is minimum at 45° direction. Therefore the resistance to creep deformation is smallest in 45° off-axis specimens, resulting in the highest creep response at the same specimens. The creep compliance is defined as the creep strain divided by the applied stress. Here, the creep compliance is made up of time-independent and dependent components. The time independent compliance indicates the initial compliance, whereas the time dependent one is obtained by subtracting the time-independent compliance from the total compliance. The time dependent compliance is shown in Fig. 4, indicating that the creep compliance of the CTM shows anisotropic and nonlinear characteristics.

As formulated in Sections 2.1 and 2.2, anisotropic and nonlinear creep behavior can be described by defining a creep potential in Eq. (1) with three orthotropic material parameters. If the material parameters in the potential are properly determined using Eq. (9), each compliance (i.e. 0°, 45°, and 90°) at each load level can be collapsed onto the master compliance curve. For 0.5 MPa level, the effective creep compliance was determined from each off-axis creep compliance as shown in Fig. 5a through minimizing Eq. (9) (see Fig. 5b). The same tendency can be observed for other two large load case (see Fig. 6). The orthotropic material parameters determined from three different creep load are plotted in Fig. 7, showing that a_{11} and a_{12} increase slightly as the stress increases, whereas a_{66} does

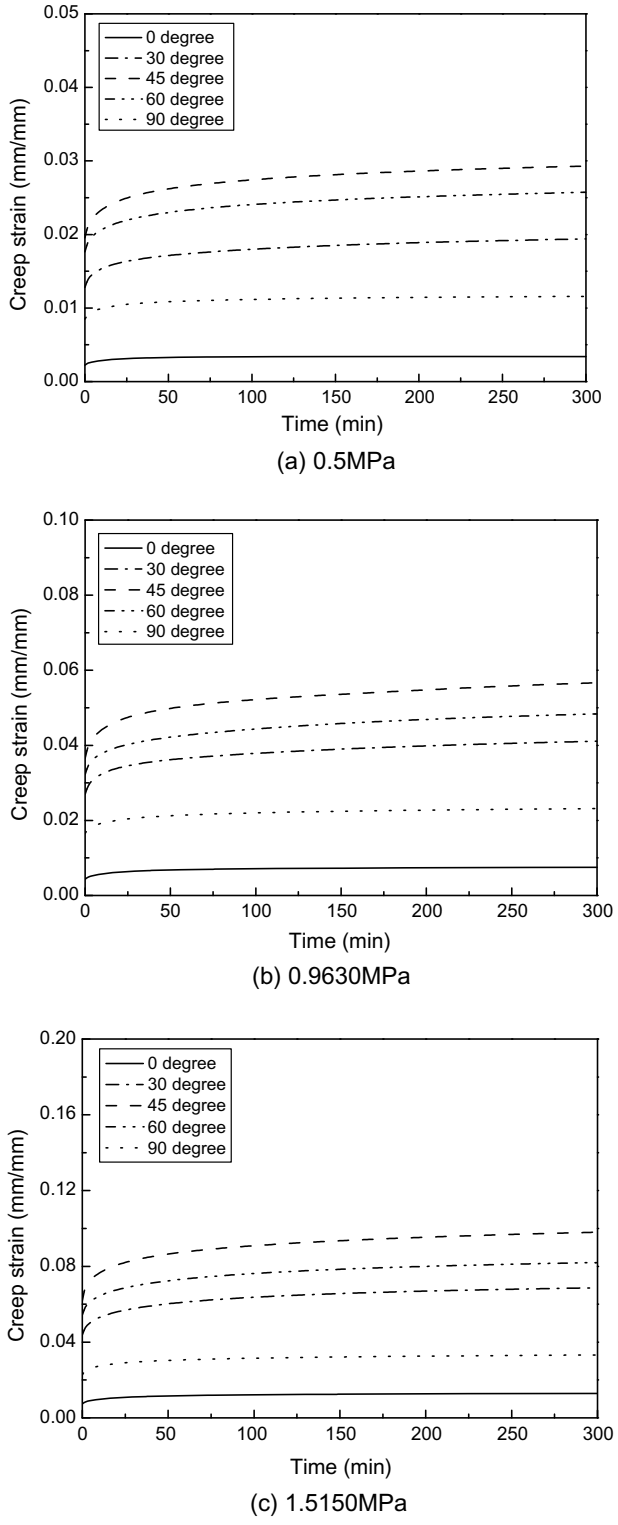

Fig. 3. Experimental creep curves of three off-axis specimens according to stress level.

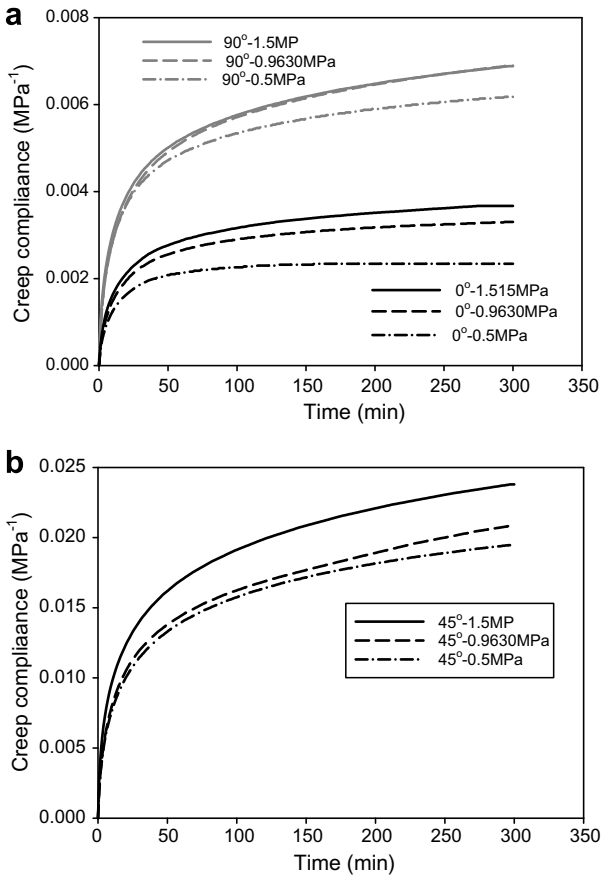

Fig. 4. Experimental creep compliance of three off-axis specimens excluding time-independent compliance; (a) 0° and 90°, (b) 45°.

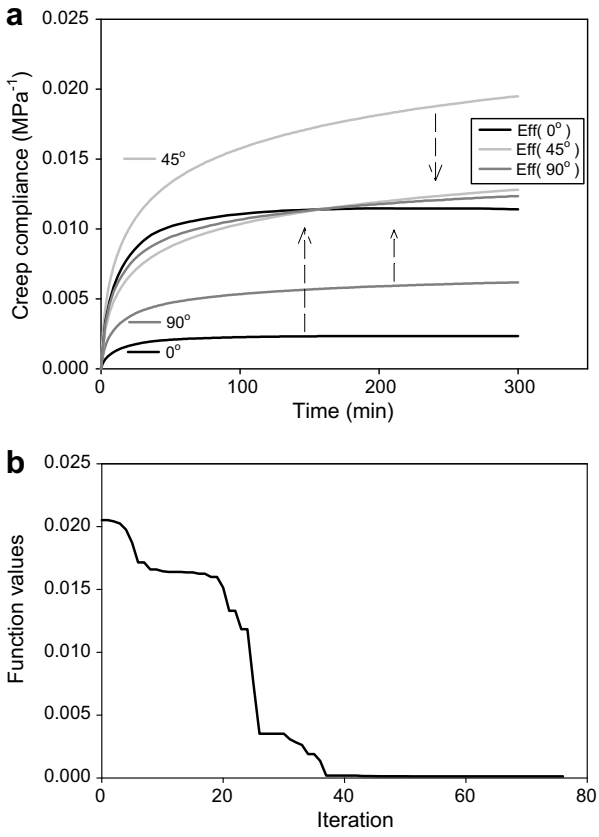

Fig. 5. Creep compliance at 0.5 MPa load level; (a) effective creep compliance from each off-axis creep compliance, (b) minimization of the objective function in Eq. (9).

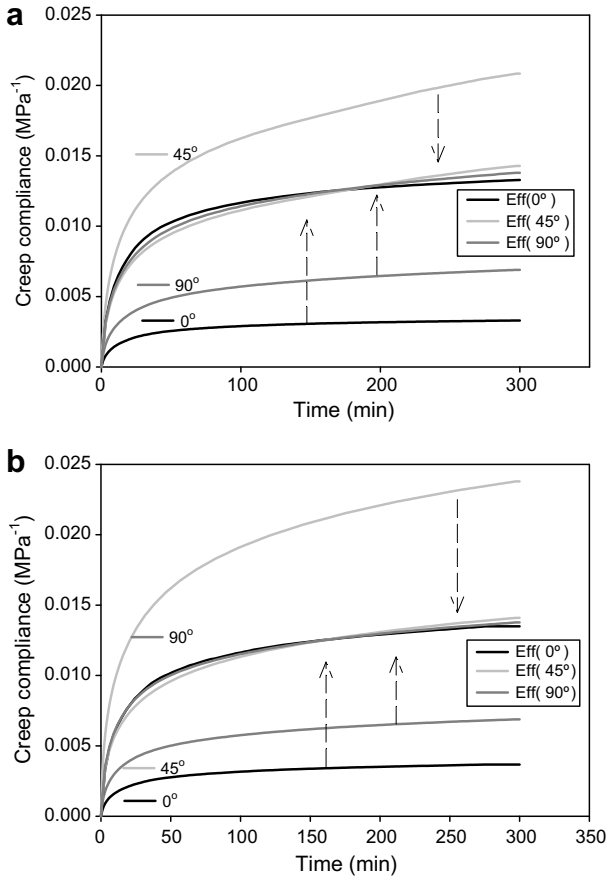

Fig. 6. Effective creep compliance constructed from each off-axis creep compliance (a) at 0.9630 MPa, and (b) 1.515 MPa.

not show any monotonic trends. It is clear that a_{66} value is the largest among the orthotropic parameters, implying that the creep strain of the woven reinforced composite is dominated by the in-plane shear mechanism.

To check the validity of the current method to determine the orthotropic material parameters (a_{11}, a_{66}, and a_{12}) using 0°, 45°, and 90° off-axis specimen, other two sets, (0°, 30°, 90°) and (0°, 60°, 90°), were also selected to determine the three material parameters using the same minimization scheme above. Results from these two sets of off-axis specimens are illustrated in Fig. 8 by plotting the effective creep stress contour (in Eq. (1)). The results show that for the low shear stress the contour does not change severely; however it shows variation as the shear stress increases, indicating that the current method for determining three orthotropic parameters is valid for moderate stress cases.

The effective creep strain rate is needed to complete the constitutive equation in Eq. (10). In this study, a simple form of the effective creep strain rate of the power law type was adopted as follows:

$$\varepsilon^{c} = A\sigma^{m}t^{n}, \quad \dot{\varepsilon}^{c} = nA\sigma^{m}t^{n-1} \tag{20}$$

where the coefficients A, m, and n are determined by fitting the experimental curve, as shown in Fig. 9. The creep strain

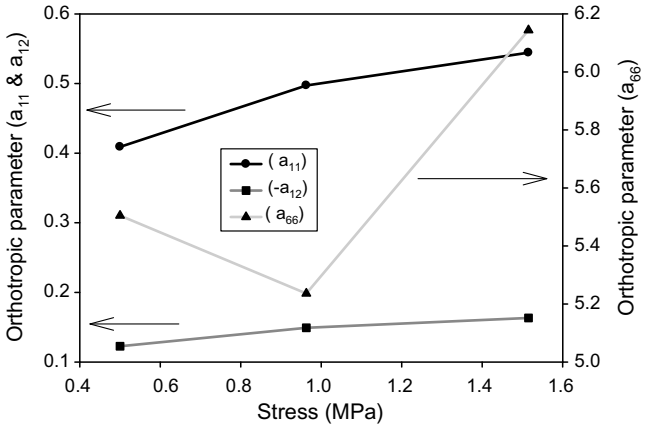

Fig. 7. Orthotropic material parameters determined from three different creep loads.

obtained from the 90 degree specimen test was used for fitting the creep equation (see Table 2 for the coefficient), which can be extended for the effective creep strain using Eqs. (6) and (7), i.e.

$$\bar{\varepsilon}^{c} = \bar{A}\bar{\sigma}^{m}t^{n}, \quad \dot{\bar{\varepsilon}}^{c} = n\bar{A}\bar{\sigma}^{m}t^{n-1} \tag{21}$$

where $\bar{A} = A/H(90^{\circ})^{m+1}$.

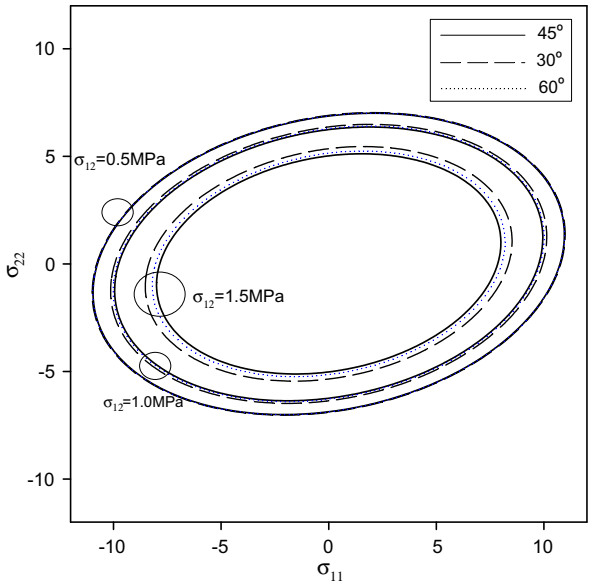

Fig. 8. Contour of the effective creep stress with three orthotropic parameters determined using different off-axis angle specimen with a creep stress of 0.5 MPa. The legend indicates an off-axis angle specimen included in a set with 0 and 90 off-axis angle specimen.

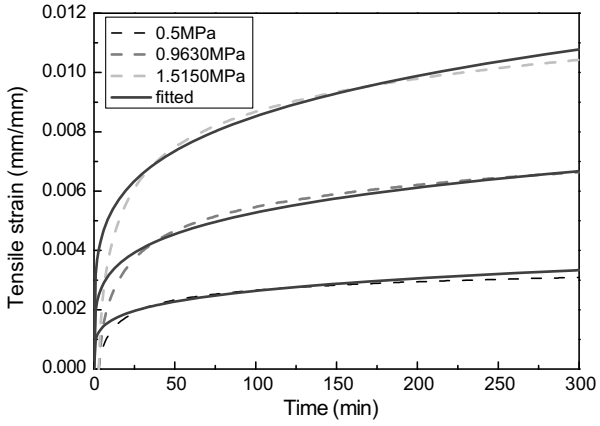

Fig. 9. Fitted creep law using results from 90° off-axis creep test.

Table 2
Orthotropic material parameters and coefficients used for creep equation

Load (MPa)	Parameters			A ($MPa^{-m}\,s^{-n}$)	m	n
	a_{11}	a_{12}	a_{66}			
0.5	0.4090	−0.1227	5.5048			
0.9630	0.4972	−0.1492	5.2362	0.00418	1.05835	0.21362
1.5150	0.5443	−0.1633	6.1438			

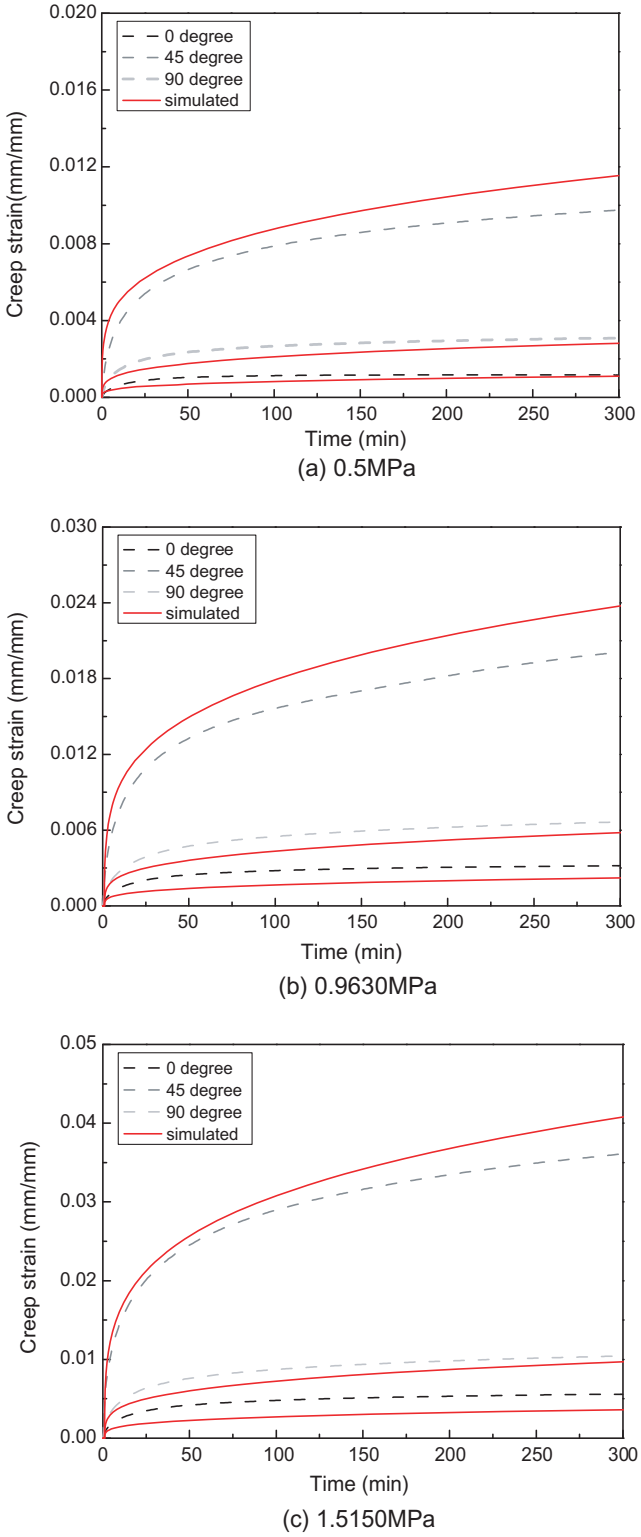

Fig. 10. Comparison of simulated creep strain with experimental one for three creep stresses with $a_{11} = 0.4090$, $a_{12} = -0.1227$ and $a_{66} = 5.5048$.

3.2. Simulation of creep behavior of CTM

To simulate the creep behavior of the CTM, the numerical formulation in Section 2.2 was implemented in finite element software (here ABAQUS/implicit) using a user material subroutine. To investigate the validity of the creep model used in this study, the uniaxial creep tests were re-simulated using shell elements (50 × 50 S4R in ABAQUS). The fixed boundary condition was imposed to one end of

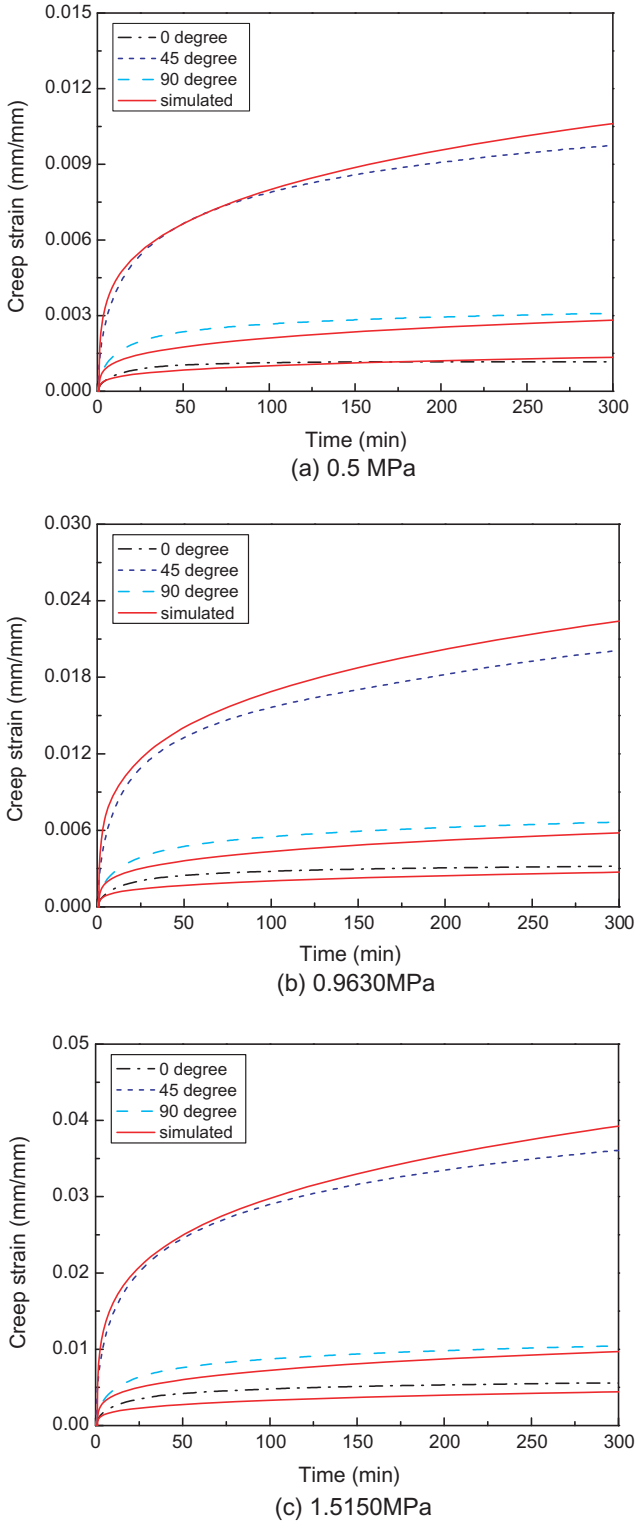

Fig. 11. Comparison of simulated creep strain with experimental one for three creep stresses with $a_{11} = 0.4972$, $a_{12} = -0.1492$ and $a_{66} = 5.2362$.

the specimen, while a uniform distributed load (the same load as that employed in the experiments) was applied to the other end. As regards the material properties, the elastic moduli in Table 1 and the orthotropic material parameters for the creep potential in Table 2 were used.

The predicted creep behavior of the CTM is compared with the experimental results in Figs. 10 and 11. The orthotropic material parameters in the creep potential (see Table 2), which was determined based on the creep experiments with a constant stress of 0.5 MPa, were used for the simulation in Fig. 10. The simulation results show that the current creep model describes the creep behavior of the CTM appropriately, in particular its anisotropic behavior, however, some discrepancy between the experiments and simulation is observed. In the 0° and 90° directions, the simulation results underestimate the creep strain, while they overestimate it in the 45° case. This tendency remains unchanged as the creep load increases. To investigate the effect of the orthotropic material parameters on the creep strain, a series of simulations were carried out. As in the previous simulation, the uniaxial creep tests were re-simulated, but the orthotropic parameters, which were determined based on a creep load of 0.9630 MPa, were used, keeping the other conditions such as the mesh and boundary condition fixed. The simulation results are compared with the experimental ones in Fig. 11, showing that an improvement in the accuracy was achieved, especially in the case of the creep strain in the 45° direction. This improvement was due to the smaller value of a_{66} in the latter simulation. The orthotropic parameter a_{66} determines the shear creep strain (see Eq. (3)). In the first simulation, it was observed that the simulation results overestimated the creep strain in the 45° direction. Since the tensile deformation in the 45° direction is closely related to the shear strain, a smaller creep strain in the 45° direction would be expected to be observed with the smaller value of a_{66}. The creep strain in the 0° direction increased in the second simulation, due to the large value of a_{11}. Note that there is no remarkable change in the 90° direction, because a_{12} in the second simulation is close to the value used in the first simulation.

It seems that the simulation results deviate from the experimental ones further as time goes by, especially in the 45 degree case (see Fig. 11). This may be due to the assumed creep equation, i.e., the power law type of creep equation (see Eqs. (20) and (21)). In the current study, the creep behavior of the CTM was assumed to be described by a power law equation, however the comparison between the simulation and experimental results indicates that the creep strain rate in the experiments is not as steep as the one in the simulation, implying that a creep equation of the power law type may be not appropriate for describing the creep behavior of the CTM. Therefore, it may be expected that another type of exponential law would describe the creep behavior of the CTM better than the power law model.

4. Conclusions

The anisotropic and nonlinear creep behavior of coated textile membranes was analyzed using the creep potential incorporated into finite element software through a user

material subroutine, for which a numerical formulation for the stress integration and material stiffness update was developed. A characterization method using off-axis creep tests and a minimization algorithm was proposed to determine the orthotropic material parameters in the creep potential. The developed constitutive equation was validated by comparing the finite element simulation of the uniaxial creep tests with the experiments. It was demonstrated throughout the simulations that the current creep model based on the 'an equation of state' approach can be utilized to effectively design moderate span enclosures such as roofs and air-halls from coated textile membranes.

Acknowledgement

The authors of this paper would like to thank the Korea Science and Engineering Foundation (KOSEF) for sponsoring this research through the SRC/ERC Program of MOST/KOSEF (R11-2005-065).

References

[1] Chilton J, Velasco R. Applications of textile composites in the construction industry. In: Long AC, editor. Design and manufacture of textile composites. Cambridge: Woodhead Publishing Limited; 2005. p. 424.
[2] Kraus H. Creep analysis. New York: John Wiley & Sons; 1980.
[3] Chung I, Sun CT, Chang IY. Modeling creep in thermoplastic composites. J Compos Mater 1993;27(10):1009–29.
[4] Hu H, Sun CT. The characterization of physical aging in polymeric composites. Compos Sci Technol 2000;60(14):2693–8.
[5] Sun CT, Chen JL. A simple flow rule for characterizing nonlinear behavior of fiber composites. J Compos Mater 1989;23(10):1009–20.
[6] Ferry JD. Viscoelastic properties of polymers. Toronto: John Wiley & Sons, Inc.; 1980.
[7] Riande E, Diaz-galleja R, Prolongo MG, Masegosa RM, Salom C. Polymer viscoelasticity-stress and strain in practice. CRC; 1999.
[8] Wineman AS, Rajagopal KR. Mechanical response of polymers. Cambridge: Cambridge University Press; 2000.
[9] Schapery RA. On the characterization of nonlinear viscoelastic materials. Polym Eng Sci 1969;9(4):295–310.
[10] Papanicolaou GC, Zaoutsos SP, Kontou EA. Fiber orientation dependence of continuous carbon/epoxy composites nonlinear viscoelastic behavior. Compos Sci Technol 2004;64(16):2535–45.
[11] Pramanick A, Sain M. Temperature-stress equivalency in nonlinear viscoelastic creep characterization of thermoplastic/agro-fiber composites. J Thermoplast Compos 2006;19:35–60.
[12] Muliana AH, Haj-Ali RM. Nested nonlinear viscoelastic and micromechanical models for the analysis of pultruded composite materials and structures. Mech Mater 2004;36(11): 1087–110.
[13] Poon H, Ahmad MF. A Finite element constitutive update scheme for anisotropic, viscoelastic solids exhibiting non-linearity of the shapery type. Int J Numer Mech Eng 1999;46:2027–41.
[14] Sawant S, Muliana A. A thermo-mechanical viscoelastic analysis of orthotropic materials. Compos Struct 2008;83:61–72.
[15] Kenaga D, Doyle JF, Sun CT. The characterization of boron/aluminum composite in the nonlinear range as an orthotropic elastic–plastic material. J Compos Mater 1987;21(6):516–31.
[16] Kachanov LM. Fundamentals of the theory of plasticity. Moscow: Mir Publishers; 1974.
[17] Sun CT, Chung I, Chang IY. Modeling of elastic–plastic behavior of LDF(TM) and continuous fiber reinforced AS-4/PEKK composites. Compos Sci Technol 1992;43(4):339–45.
[18] Thiruppukuzhi SV, Sun CT. Models for the strain-rate-dependent behavior of polymer composites. Compos Sci Technol 2001;61(1): 1–12.
[19] Yu W-R, Kim MS, Lee JS. Modeling of anisotropic creep behavior of coated textile membranes. Fiber Polym 2006;7(2):123–8.
[20] Belytschko T, Liu WK, Moran B. Nonlinear finite elements for continua and structures. Chichester: John Wiley & Sons, Ltd.; 2001.
[21] Kojic M, Bathe KJ. Inelastic analysis of solids and structures. Springer; 2005.